Statistical Characterization of Zonal and Meridional Ocean Wind Stress

SARAH T. GILLE

Scripps Institution of Oceanography, and Department of Mechanical and Aerospace Engineering, University of California, San Diego, La Jolla, California

(Manuscript received 9 November 2004, in final form 6 January 2005)

ABSTRACT

Four years of ocean vector wind data are used to evaluate statistics of wind stress over the ocean. Raw swath wind stresses derived from the Quick Scatterometer (QuikSCAT) are compared with five different global gridded wind products, including products based on scatterometer observations, meteorological analysis winds from the European Centre for Medium-Range Weather Forecasts, and reanalysis winds from the National Centers for Environmental Prediction. Buoy winds from a limited number of sites in the Pacific Ocean are also considered.

Probability density functions (PDFs) computed for latitudinal bands show that mean wind stresses for the six global products are largely in agreement, while variances differ substantially, by a factor of 2 or more, with swath wind stresses indicating highest variances for meridional winds and for zonal winds outside the Tropics. Higher moments of the PDFs also differ. Kurtoses are large for all wind products, implying that PDFs are not Gaussian. None of the available gridded products fully captures the range of extreme wind events seen in the raw swath data.

Frequency spectra for the five gridded products agree with frequency spectra from swath data at low frequencies, but spectral slopes differ at higher frequencies, particularly for frequencies greater than 100 cycles per year (cpy), which are poorly resolved by a single scatterometer. In the frequency range between 10 and 90 cpy that is resolved by the scatterometer, spectra derived from swath data are flatter than spectra from gridded products and are judged to be flatter than $\omega^{-2/3}$ at all latitudes.

1. Introduction

Scatterometry has revolutionized our ability to gather vector wind measurements over the ocean. Global measurements started with *Seasat*, which provided three months of measurements in the late 1970s. *Seasat* was followed in the 1990s by the narrow swath scatterometer abroad the European Space Agency's *Earth Remote Sensing-1/2* (*ERS*) satellites and by the short-lived National Aeronautics and Space Administration (NASA) Scatterometer (NSCAT), which operated for nine months in 1996–97. The SeaWinds instrument aboard the Quick Scatterometer (QuikSCAT) satellite was launched in 1999 and has now generated more than 4 yr of wind measurements over the global ocean, providing an unprecedented view of wind variability, particularly in regions where there are few shipping routes and where in situ samples are difficult to obtain, such as the Southern Ocean.

QuikSCAT's antenna scans an 1800-km-wide swath, so that it is able to measure winds at least once per day over most of the planet. QuikSCAT follows a sun-synchronous orbit. For ascending satellite passes, the nadir beam measures at approximately 0600 UTC; for descending passes, measurements are centered around 1800 UTC. Sampling is densest at high latitudes, where satellite overpasses occur almost every 12 h. Near the equator, the swath coverage is less complete, and gaps of 24 to 36 h may occur between wind measurements. Comparisons between QuikSCAT and ship and buoy winds show excellent agreement over a broad range of wind speeds (QuikSCAT Project 2000; Pickett et al. 2003; Bourassa et al. 2003).

Ocean surface winds provide information about the boundary layer atmosphere and the forcing that drives the ocean. They are used to investigate the ocean response to wind forcing and to drive ocean circulation models. Many of these applications require regularly spaced wind fields. A number of efforts have been

Corresponding author address: Dr. Sarah T. Gille, Scripps Institute of Oceanography, University of California, San Diego, La Jolla, CA 92093.
E-mail: sgille@ucsd.edu

made to produce gridded wind products, from scatterometer winds and from other atmospheric observations. Scatterometer mapping algorithms often average several days or even weeks of data in order to minimize the "trackiness" associated with the swath sampling of the satellite tracks. These mapping algorithms smooth over noise, which may be due to measurement errors, or in regions of rapid temporal or spatial variability may represent physically important components of the wind fields. Ground truth data with high resolution in both time and space are not available, and the extent to which mapping may suppress physically relevant details of the winds is not known.

This study evaluates the skill with which the gridded wind products are able to capture the basic statistical properties of the wind stress variability seen by the scatterometer. Wind stresses are specifically considered rather than wind velocities, because wind stress is the quantity that drives ocean circulation. This analysis covers all latitudes between 60°S and 60°N. Regions poleward of 60° are excluded because the high incidence of ice cover limits scatterometer coverage near the poles. A number of previous studies have used numerical weather prediction analyses to look at cyclones and storm systems (e.g., Sinclair 1994; Simmonds and Keay 2000) or have examined the large-scale spatial structure of the winds with empirical orthogonal functions (Levy 1994). The approach of this study differs from these past investigations, because here the emphasis is on characterizing the statistics that describe the zonal and meridional components of the Eulerian wind stresses. Probability density functions and frequency spectra are used to describe the basic structure of wind variability. These are particularly relevant for ocean models that seek to understand the ocean response to stochastic wind forcing with known statistical characteristics (e.g., Sura and Penland 2002; Weijer 2005) or that evaluate the response of ocean circulation to high-frequency, high-wavenumber wind variability (e.g., Milliff et al. 1996; Chen et al. 1999; Milliff et al. 1999).

Section 2 describes the data used for this analysis. Section 3 presents means, variances, and higher moments computed from probability density functions (PDFs), and section 4 presents frequency spectra computed from both gridded and swath wind stress fields. Results, summarized in section 5, indicate that the mean fields and low frequency variability are largely in agreement for the six wind products examined here. However, swath wind stresses have flatter spectral slopes than gridded products and contain more extreme events, which influences the higher moments of the PDFs.

2. Wind data types

The analysis reported in this paper makes use of swath winds as well as five global gridded wind products. All represent the 4-yr period, 1 September 1999–31 August 2003, corresponding roughly to the first 4 yr of the QuikSCAT mission. Figure 1 shows snapshots plots of all six wind fields in the Drake Passage region for 1 July 2000. (Drake Passage is shown in these comparison maps because of its strong and variable winds.)

Swath winds (Fig. 1a) are derived from level 2B winds at 25-km resolution, based on Remote Sensing Systems' Ku2001 algorithm [available online at remss.com; Wentz et al. (2001)]. The Ku2001 winds were selected, because they performed better than winds derived from the Jet Propulsion Lab (JPL) QSCAT-1 algorithm in comparisons with ship observations (Bourassa et al. 2003). In the Southern Ocean, Yuan (2004) found no significant bias between the Ku2001 winds and in situ meteorological observations at Macquarie Island. However, she noted that the Ku2001 fields indicated more frequent extreme events than QSCAT-1 fields. The higher moment statistics computed in this study are likely to be sensitive to this difference. Wind locations are determined relative to the satellite ground track, and no mapping procedure is applied. The satellite design requirements specified speed accuracy of 2 $m\,s^{-1}$ or 10% and directional accuracy of 20° (Lungu 2001). Comparisons of Ku2000 winds (the precursors to Ku2001) with winds measured from research ships within 12.5 km in space and 30 s in time indicate 3° directional accuracy and 0.3 $m\,s^{-1}$ speed accuracy in rain-free conditions once wind directional ambiguity errors were eliminated (Bourassa et al. 2003). The scatterometer is less well calibrated for high wind speeds, because in situ wind measurements are difficult to obtain under extreme conditions, although hurricane wind observations have helped to improve the wind model function. Swath winds have greater directional errors at the outer edges of the swath and along the nadir beam than in the so-called sweet spots located in the central region between the nadir and swath edge. QuikSCAT SeaWinds data are released with a composite rain flag, and in this analysis, all rain flagged data are rejected. In a careful analysis of the impact of rain on scatterometer fields, Milliff et al. (2004) noted that wind stress curl and divergences can be biased by the rejection of winds measured under strong rain conditions, such as occur in cyclones. For this study, swath winds have not been mapped, and therefore no mapping biases or errors have been introduced into the data. Because the data

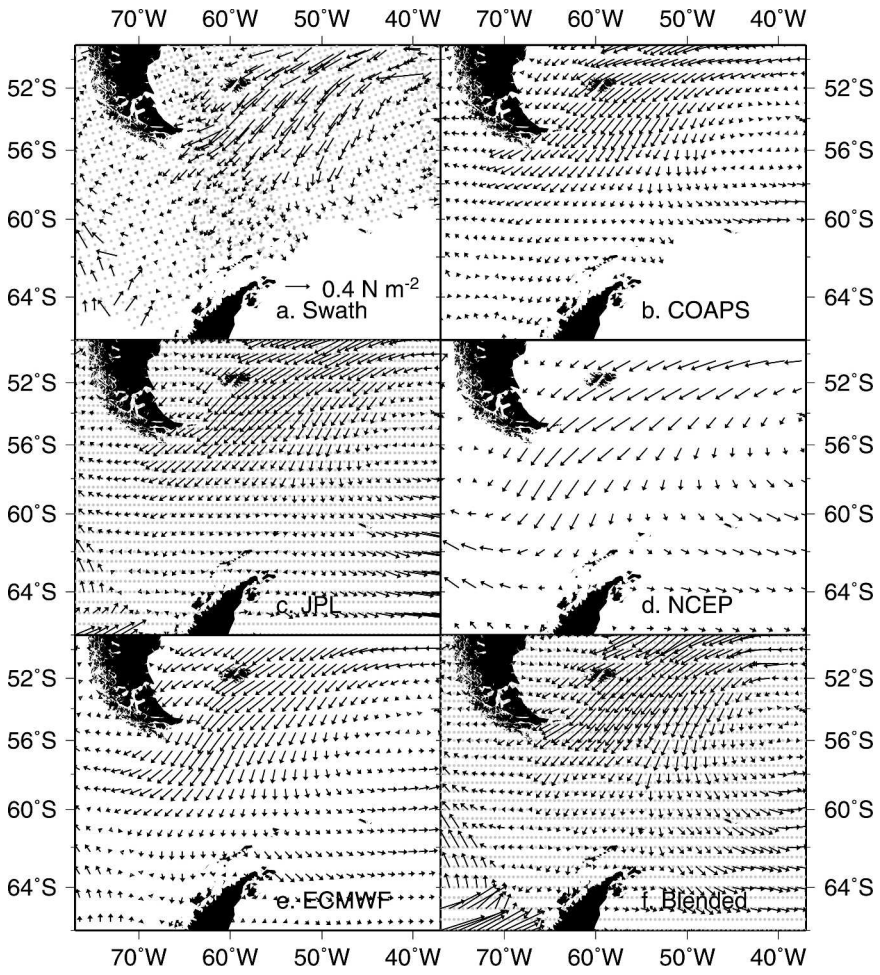

FIG. 1. Vector wind stress fields used in this study from the Drake Passage region. Gridded winds represent the first available sample for 1 Jul 2000 (UTC). Swath winds show vectors from the first 12 h of the day. For swath winds, roughly one-sixteenth of the vectors are drawn, and one-quarter are indicated with gray dots. For JPL and blended winds, one-quarter of the vectors are drawn, and the remaining data points are indicated with gray dots. (a)–(f) The six wind products show similar large-scale patterns.

have not been smoothed, they may have greater random errors than smoothed and gridded data.

The swath winds were compared with two gridded products derived from QuikSCAT observations, with two fields derived from meteorological forecast models, and with one blended product that merges reanalysis winds with QuikSCAT observations. The wind products used here were selected because they are readily available for the 4-yr study period and have been generated using documented algorithms. They do not represent a definitive list of gridded wind fields.

One gridded product is produced by Florida State University's Center for Ocean–Atmospheric Prediction Studies (COAPS; Fig. 1b). Pseudostress values are mapped at 6 h by 1° by 1° resolution by iteratively minimizing a cost function that smooths the winds and requires the gridded values to match the available scatterometer observations and to have a curl that resembles the curl of a smoothed background field (Pegion et al. 2000; M. Bourassa 2004, personal communication). Rain-contaminated values are excluded from the analysis.

A second gridded product (Fig. 1c) is produced by the Jet Propulsion Laboratory from near-real time wind vectors provided by the National Oceanic and Atmospheric Administration (NOAA; Tang and Liu 1996; Liu et al. 1998). This wind field has 12-h temporal resolution and half-degree spatial resolution.

Two different numerical weather prediction analysis winds were considered. The National Centers for Environmental Prediction–National Center for Atmospheric Research (NCEP–NCAR) reanalyzes available

meteorological observations to produce a consistent climatological record (Fig. 1d). The reanalysis project uses the 1995 version of the NCEP model, with a 3D variational analysis scheme (Kalnay et al. 1996; Kistler et al. 2001). The NCEP operational model began assimilating 1° resolution QuikSCAT winds 15 January 2002 (Yu 2003), but the NCEP–NCAR reanalysis project reports no plans to incorporate QuikSCAT data into their product. Winds are available at 6 h by ~1.9° latitude by 1.875° longitude resolution. Since scatterometer winds are excluded under rainy conditions, NCEP reanalysis precipitation rates were used to allow comparisons of all-weather and rain-free winds. However, rain data are not assimilated into the NCEP analysis, so NCEP rain estimates may be of questionable quality. Therefore, comparisons based on NCEP precipitation rates should be interpreted with caution.

A second numerical weather prediction product comes from the European Centre for Medium-Range Weather Forecasts (ECMWF; Fig. 1e). This model has used a four-dimensional variational assimilation scheme since November 1997 to assimilate a broad range of meteorological observations (Rabier et al. 2000). Previous studies have indicated that 1990s ECMWF winds are better correlated than NCEP winds with Southern Ocean bottom pressure (Gille et al. 2001) and surface drifter observations (Elipot and Gille 2002). For the present study, 6 h by 1.125° by 1.125° gridded analysis fields were used. Since 22 January 2002, ECMWF has assimilated QuikSCAT winds. This has improved forecasts, particularly in the Southern Hemisphere (Hersbach et al. 2003), which may alter the comparison statistics for this study. ECMWF also has produced reanalysis products, but they were not used here, because the reanalyses terminate before the end of this study period.

Finally, a blended product (Fig. 1f) was examined. QuikSCAT provides measurements at only 2 times per day (at best), while many applications are tuned to take advantage of more frequent winds, such as the 6-hourly numerical weather prediction fields. The blended product merges the high-wavenumber information available from observations with high-frequency numerical weather prediction fields (Chin et al. 1998; Milliff et al. 1999). The method uses the spectral properties of the observed winds to synthesize high-wavenumber winds at times and locations where no observations exist. R. F. Milliff and J. Morzel (2001, personal communication) have released fields based on QuikSCAT winds and NCEP reanalysis with 6-h temporal resolution and 0.5° spatial resolution. This reanalysis uses their version 4 product, released in 2003.

All wind products provide winds at 10-m elevation and all represent velocity $\mathbf{u}$ (m s^{-1}), with the exception of COAPS, which is in pseudostress, equivalent to wind speed multiplied by wind velocity $|\mathbf{u}|\mathbf{u}$ (m^2 s^{-2}). For this study all wind products have been converted to wind stress, $\boldsymbol{\tau}$, where $\boldsymbol{\tau} = \rho_a C_d |\mathbf{u}|\mathbf{u}$. Here ρ_a, the density of air, is assumed to be 1.2 kg m^{-2}. The drag coefficient C_d found by Yelland et al. (1998) is used for winds between 6 and 26 m s^{-1}, and the coefficient of Yelland and Taylor (1996) for winds between 3 and 6 m s^{-1}. Outside of this range, drag coefficients are fixed as constants to match the end points of the fitted coefficients. Mestas-Nuñez et al. (1994) made a similar choice for low wind speeds, and hurricane observations by Powell et al. (2003) support the use of a constant C_d at high wind speeds. The NCEP, ECMWF, and blended wind fields, which provide data over land as well as the ocean, have been masked out over land so that the comparison statistics are the same for all wind products.

Buoy measurements routinely provide ground truth for satellite wind observations (e.g., Freilich and Dunbar 1999). Kelly et al. (2001) noted that scatterometer winds may appear biased relative to buoy observations, because moored buoys detect absolute wind, while scatterometers measure wind relative to surface currents. Buoy winds and scatterometer winds can also differ, because waves influence surface turbulent stress in the ocean (Quilfen et al. 2001; Bourassa 2004). In general, scatterometer measurements correspond to winds that actually drive the ocean. In most locations outside the Tropics or western boundary currents, the difference between buoy and scatterometer winds is likely to be small, because mean winds are large compared with upper ocean currents (although wave effects may still lead to some differences). Buoy locations are extremely limited in the Southern Hemisphere, but span a broad range of latitudes in the Tropics and the Northern Hemisphere. For this analysis, winds from 70 noncoastal buoys from the Pacific Ocean were selected for comparison, as depicted in Fig. 2. Each provides a multiyear record of wind at hourly intervals. Hourly winds were used rather than high-frequency 10-min winds, because high-frequency wind and temperature observations were not available at all locations.

Most buoys measure winds at 4- or 5-m elevation, while scatterometer data are calibrated to represent 10-m equivalent neutral winds, and weather service wind products normally report 10-m winds. Therefore, buoy winds were converted to equivalent neutral winds at 10-m elevation following Liu et al. (1979) and Liu and Tang (1996) and transformed to represent wind stress.

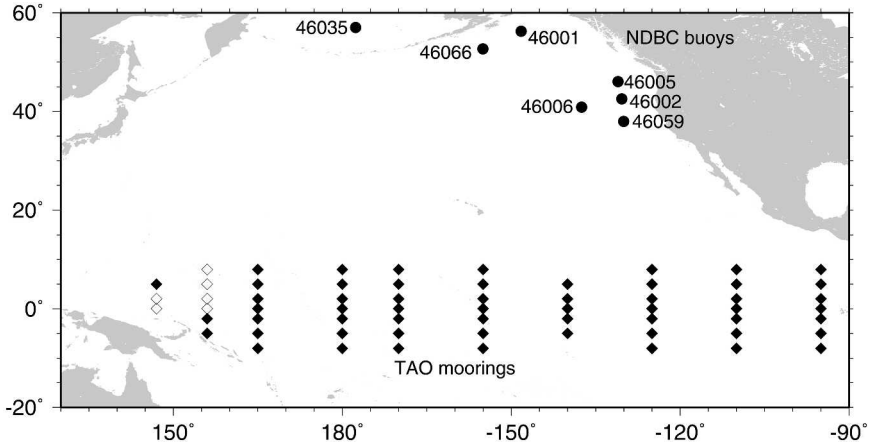

FIG. 2. Locations of buoys with multiyear wind records used for comparison in this study. A total of 63 tropical buoys come from the TAO Project; these report winds at 4-m elevation. Of the TAO buoys, 57 (solid black diamonds) overlapped in time with QuikSCAT; others (white diamonds) were used to provide regional statistics. Seven extratropical buoys (black circles) from the NDBC were also used. Most of these collected wind observations at 5-m elevation, with the exception of Station 46035 at 57.05°N, 177.58°W, which measures 10-m winds.

3. Probability density functions: Characterizing extreme events

Probability density functions (PDFs) of wind stress measure the empirical likelihood of observing a particular value. For this study, PDFs are used to estimate the mean, variance, skewness, and kurtosis of the wind fields. This differs from some previous applications of PDFs for scatterometry, which have looked at wind speed (rather than vector wind stress) in order to derive improved model functions and to quality control data (e.g., Freilich and Challenor 1994; Bauer 1996; Ebuchi 1999). Extreme events may occur in one data product but not others, because anomalous events are edited out of some data products.

Figure 3 shows PDFs of the zonal and meridional

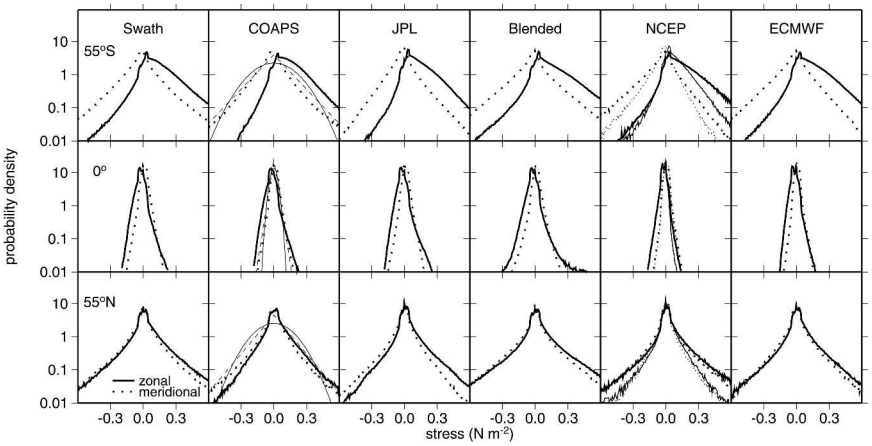

FIG. 3. PDFs of wind stress at (top) 55°S, (middle) 0°, and (bottom) 55°N for the six wind products considered in this analysis. Zonal winds are indicated with solid lines and meridional winds with dotted lines. These PDFs compile all data collected within a 1°-wide latitude band (1.12° for ECMWF; 1.9° for NCEP) between 1 Sep 1999 and 31 Aug 2003. For reference, in the COAPS panels, thin solid and dashed lines represent Gaussian and double exponential distributions, respectively. Thin lines for NCEP winds show results obtained under zero precipitation conditions, in analogy with the scatterometer rejection of winds obtained during rain.

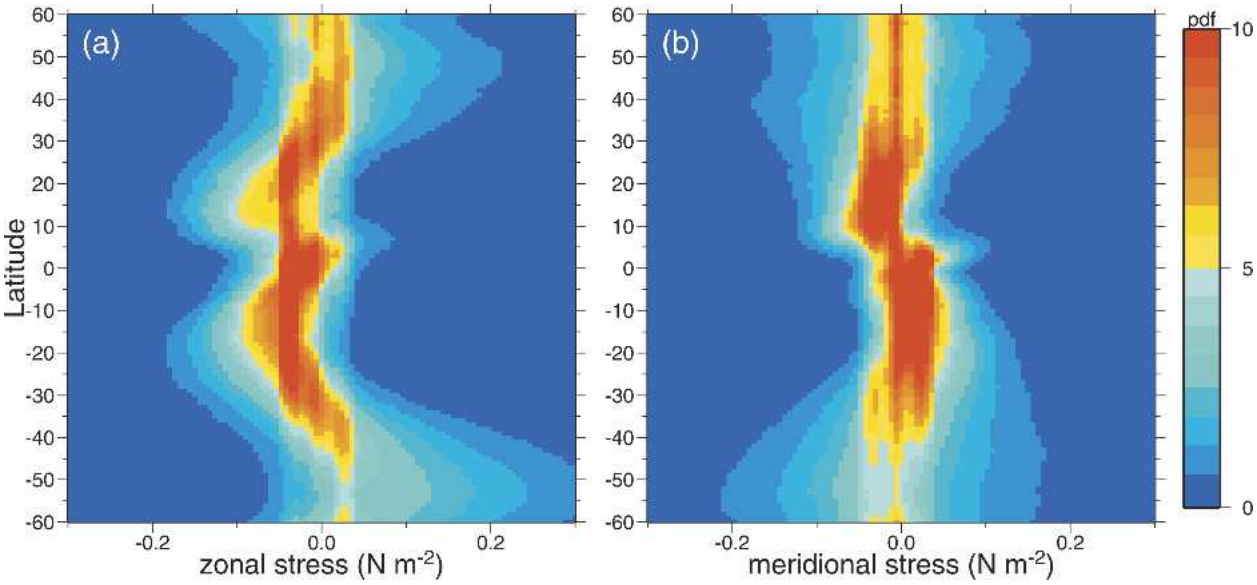

FIG. 4. Swath wind stress PDFs: (a) the zonal component and (b) the meridional component as a function of latitude. PDFs are computed by combining wind stresses over the ocean from all longitudes, sorted in 1° latitude bins for the 4-yr period between 1 Sep 1999 and 31 Aug 2003.

components of wind stress from the six wind fields used in this study at 55°S, the equator, and 55°N. PDFs are plotted on a logarithmic scale. The decision to combine data in zonal bins for this analysis was motivated by the fact that the dominant wind belts are zonal, so wind statistics are expected to vary less in the zonal direction than in the meridional direction. By merging all data at each latitude, we obtain enough data points to compute robust statistics. All six products agree in basic structure. In the Southern Ocean, zonal wind stresses are skewed eastward, as expected because of the strong westerly winds of the region, while meridional wind stresses are generally more symmetric. At 55°N, both the meridional and zonal wind stress components have broad peaks near zero stress and wide tails. At the equator winds have smaller variances and the PDFs are correspondingly narrower, though the blended winds show high incidence of large positive wind stress events. Although geophysical quantities are often hypothesized to have normal or Gaussian distributions, neither the zonal nor the meridional components of the wind resemble a Gaussian distribution (indicated by thin solid lines in the COAPS wind panels). For example, at 55°S, the meridional PDFs are characteristic of double exponential distributions (indicated by thin dashed lines), while the skewed structure of the zonal wind stresses make them more difficult to characterize.

Despite the large-scale similarities, specific details of the six wind products in Fig. 3 differ. The JPL wind stresses have narrower distributions than other products implying a lower variance. JPL, blended, NCEP, and ECMWF zonal wind stresses have pronounced peaks at zero wind stress. A more detailed investigation of the wind statistics (not shown) indicates that these peaks at zero are associated with longitudinal variations in wind distributions. For example, wind stresses near Drake Passage tend to have smaller means and less variability than wind stresses in the more open portion of the Southern Ocean. In contrast, COAPS gridded wind stresses have a smoother distribution near zero wind stress than other products.

a. Latitudinal variations of PDFs

Figure 4 shows swath wind stress PDFs as a function of latitude for the zonal (Fig. 4a) and meridional (Fig. 4b) components of the wind. The vertical bands in the plot do not appear in the PDFs for wind velocity components or pseudostress (not shown) and are a direct result of the nonlinearities in the drag coefficient used to convert 10-m winds to wind stress. Meridional wind stresses in mid and high latitudes are centered around zero, and in the Tropics they indicate convergence toward the intertropical convergence zone. Zonal wind stresses peak at zero almost everywhere except in the Tropics and between 45° and 60°S, over the Antarctic Circumpolar Current. They show evidence for mean westward wind stresses in the Tropics and predominantly eastward stresses in subpolar regions. At some latitudes, such as for the zonal wind stresses between

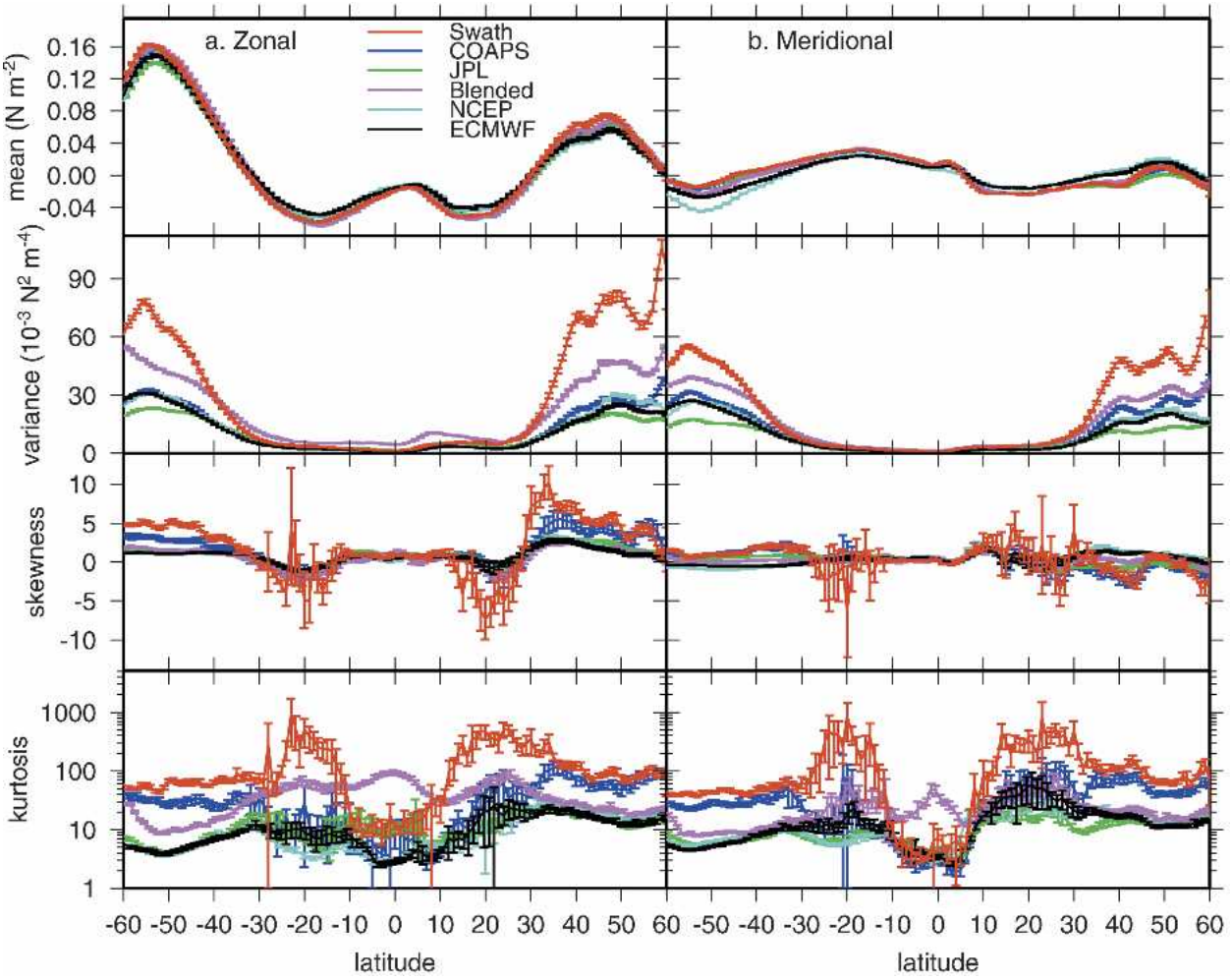

FIG. 5. First four moments of (left) zonal stress PDFs and (right) meridional stress PDFs. (top) Mean, (second) variance, (third) skewness, and (fourth) kurtosis. As in Fig. 4, PDFs represent a 4-yr period.

25° and 35°S, the PDF appears to have a double peak, with maxima at zero and at about -0.05 N m^{-2}. This occurs because wind statistics vary at different longitudes. For example, mean wind stresses and their variances are often low near land but higher in midocean regions. When data from all longitudes are combined, the resulting PDFs have double peaks.

As a function of latitude, PDFs for the five gridded wind products closely resemble the swath PDFs shown in Fig. 4 and are not shown here. Double peaks are less pronounced in the COAPS gridded wind stresses than in the other products considered in this study; this can be explained by the fact that the COAPS product is generated by mapping wind pseudostress rather than wind velocity, which results in fewer near-zero values of stress. It may also be influenced by the fact that compared with other products, COAPS winds more closely resemble 24-h averages than snapshots.

The first four moments of the PDF define the mean (μ_1), variance (μ_2), skewness ($\mu_3/\mu_2^{1.5}$), and kurtosis (μ_4/μ_2^2) of the data. Figure 5 shows these moments as a function of latitude for the six wind products. Although the swath, JPL, and blended data products are available at half degree or greater spatial resolution, these data are binned into 1° latitude bands in order to compute PDFs. For swath data, moments of PDFs are computed from the higher-quality sweet spot data only. (The scatterometer swath samples 76 columns across; for PDFs a conservative definition is used, employing only columns 10–25 and 52–67.)

For this analysis, error bars of the mean PDF moments are computed by determining the standard deviation of the observations divided by the square root of the number of degrees of freedom, N_{df}. The value of N_{df} differs from the total number of observations N that contribute to each PDF, because wind measurements

TABLE 1. Temporal and spatial increments between observations and decorrelation scales for the first four moments of the PDF at 55°S. Here, decorrelation scales are computed for powers of $u - \bar{u}$ rather than skewness and kurtosis. In essence, this treats the variance used to normalize skewness and kurtosis as a constant over the domain of interest. Decorrelation scales for swath wind stresses are estimated by first observations in 0.4° latitude by 0.4° longitude by 12-h bins

Product	Measurement time (h)	Interval space (°lat/°lon)	Time (days)				Space (° lon)			
			μ_1	μ_2	μ_3	μ_4	μ_1	μ_2	μ_3	μ_4
	Zonal									
JPL	12	0.5	3.0	1.3	1.5	1.1	28.2	12.1	12.0	7.5
Blended	6	0.5	2.1	0.7	0.8	0.6	19.7	7.5	6.0	4.1
NCEP	6	1.875	2.6	0.8	1.0	0.6	24.9	12.6	13.8	9.9
ECMWF	6	1.125	2.5	0.8	0.9	0.5	25.3	11.8	12.4	8.6
COAPS	6	1	2.3	0.8	0.8	0.5	21.7	8.6	7.4	5.1
Swath	12	0.4	1.8	0.7	0.7	0.6	15.7	5.8	4.6	3.1
	Meridional									
JPL	12	0.5	1.7	1.1	1.2	1.0	15.4	11.0	8.8	6.4
Blended	6	0.5	1.0	0.7	0.6	0.5	12.3	8.2	6.0	4.7
NCEP	6	1.9	1.1	0.6	0.6	0.4	14.1	9.6	9.2	7.1
ECMWF	6	1.125	1.1	0.6	0.6	0.4	13.7	9.8	8.2	6.4
COAPS	6	1	1.1	0.7	0.6	0.5	13.2	8.9	6.7	5.1
Swath	12	0.4	0.9	0.6	0.6	0.5	10.8	6.0	4.4	3.4

are correlated in time and space. Formally, the separation S between independent observations can be computed from $S = \Sigma_{n=-l}^{l}[1 - (|n|/l)]\rho(n)$ (e.g., Davis 1976), where $l \leq N$ and $\rho(n)$ represents the lagged covariance of the data. In reality, $\rho(n)$ is poorly determined for large n, and S varies depending on l. Here, the maximum value of S is determined separately for spatial (S_x) and temporal (S_t) lags. In most cases, S does not differ substantially from what would be obtained by determining the value of $2n$ when $\rho(n) = \rho(0)/2$. Finally, S_x and S_t are used to estimate the number of correlated observations that are likely to fall within an elliptical region defined to have axes of length S_x and S_t. Thus, $N_{\text{df}} = N/(\pi S_x S_t/4)$. Higher moments of the PDFs decorrelate more rapidly, so S_x and S_t are computed separately for each of the moments. Table 1 summarizes the decorrelation space and time scales computed for the six wind products at 55°S. Temporal and spatial variations in wind fields are not necessarily orthogonal, but spatiotemporal correlations between wind stresses have been neglected in the present calculation. Temporal decorrelation scales for the six products do not differ substantially, although JPL wind stresses tend to decorrelate most slowly, suggesting greater temporal smoothing. Spatial decorrelation scales are shortest for the swath wind stresses implying that mapping procedures impose some spatial coherence on the winds.

These decorrelation scales are applied at all latitudes, since their use in this study is merely to estimate appropriate error bars. Equatorial wind stresses can decorrelate more slowly in time than high-latitude wind stresses, but the differences were judged unlikely to bias error bars by more than about 10%.

The zonal wind PDF in Fig. 5 has a nonzero mean at most latitudes, with strong eastward flow poleward of about 40°S and westward flow in the subtropics. Meridional wind stresses indicate equatorward flow in the Tropics and subtropics and poleward flow at high latitudes. Zonally averaged means for all six products are generally in agreement within error bars, although NCEP wind stresses imply a stronger poleward flow in the Southern Hemisphere than is supported by scatterometer observations.

In the second row of panels in Fig. 5, variances for the six wind products differ by almost a factor of 2. Because data from all longitudes are combined, these variances represent a combination of spatial and temporal effects. In general, high variances occur at latitudes where wind speeds are large. The swath and blended data have consistently high variance at all latitudes, while the mapped COAPS and JPL products have less variance than the raw data. In some cases, this may occur because the mapping algorithms eliminate unrealistic outliers from the observations. The ECMWF analysis and NCEP reanalysis wind stresses both have moderate variances.

The factor of 2 difference in variance applies not only for wind stress but also for wind velocity and pseudostress, and thus may have important implications for calculations that depend on squared or cubed powers of wind speed such as air–sea gas exchange (Wanninkhof 1992; Wanninkhof and McGillis 1999) or ocean mixed-layer depth (e.g., Kraus and Turner 1967). While some air–sea gas exchange calculations make use only of the mean wind speed computed from data and assume a fixed wind speed PDF, calculations of time-varying

quantities are likely to be sensitive to the choice of wind product.

Higher moments of PDFs are inherently sensitive to small changes in data values, and should therefore be interpreted with caution when computed from data (e.g., Press et al. 1992). Skewness, a measure of the lopsidedness of the PDFs (shown in the third row of panels in Fig. 5), tends to be positive in latitudes where the mean wind velocity is positive, and negative when the mean wind is negative. Equatorward of about 20° latitude, skewness for the six wind products agrees within error bars and is not statistically different from zero. At high latitudes, zonal swath wind stresses have much higher skewness than other products, primarily because swath winds retain strong wind events exceeding 30 m s^{-1} that appear to be smoothed out of gridded products. Aspects of the nonzero skewness of the winds and related statistics have been explored in several recent studies (Sura 2003; Monahan 2004a,b).

The bottom panels of Fig. 5 show kurtosis as a function of latitude. Kurtoses differ substantially for the six wind products. Here kurtosis is defined so that a Gaussian distribution would have a kurtosis of 3, and a double-exponential distribution would have a kurtosis of 6. In the Tropics, kurtoses are near 3 for all meridional wind stresses except the blended winds and for the zonal ECMWF and NCEP wind stresses. Elsewhere PDFs appear consistently non-Gaussian. In the extratropical Southern Hemisphere, ECMWF, NCEP, and JPL wind stresses have kurtoses around 6 and other products have larger kurtoses. In the extratropical Northern Hemisphere, kurtoses consistently exceed 10. As noted by Gille and Llewellyn Smith (2000), if Gaussian observations with differing variances are grouped together, the resulting PDFs will be non-Gaussian. Since data from a broad range of longitudes have been merged, one might imagine that longitudinal variations could explain the non-Gaussian PDFs shown here. In reality, even wind PDFs from small 2.5° by 2.5° regions over the ocean tend to be non-Gaussian. The high kurtoses found here indicate infrequent extreme events, which may occur as a result of unfiltered measurement noise but may also indicate the presence of infrequent high velocities that would be expected to be associated with storms. Mapping algorithms that smooth out extreme events or that represent averages over extended time periods are expected to produce lower kurtoses than mapping algorithms that use minimal smoothing in time and space. Swath wind stresses have high kurtoses near 20°S and 20°N, which are associated with tropical storms that may be smoothed out of other wind products. Swath wind stresses also indicate high kurtosis in most of the Northern Hemisphere, which is associated with storm events that tend to occur less frequently in eastern portions of ocean basins than in central to western regions. In contrast, storms in the Southern Hemisphere are more frequent and more uniformly distributed in time and space so have less impact on the kurtosis. Some of the high wind occurrences in the swath fields may represent unflagged rain events. The high kurtosis observed near the equator in the blended wind stresses is associated with tropical storms that are reconstructed in the blended winds but are not as strong in the other products.

b. Evaluating scatterometer data quality

In Fig. 5, the disagreements between PDF moments obtained from the raw swath wind stresses and those obtained from gridded products may indicate problems with the gridded products, but they may also be caused by deficiencies in the scatterometer winds.

QuikSCAT retrievals include no data in rainy conditions. Since rainfall can coincide with strong wind conditions, such as occur in hurricanes, this might be expected to bias the scatterometer winds. To evaluate the impact of the scatterometer no rain bias, the NCEP precipitation fields were used to compare wind stresses obtained under no-rain and all-weather conditions. The light lines in Fig. 3 show that outside the Tropics, the no-rain condition results in narrower NCEP PDFs with lower variance and kurtosis. Within the Tropics, NCEP variances for all-weather and no-rain conditions do not differ significantly. [Likewise, Tropical Atmosphere Ocean (TAO) mooring data also show no difference within error bars between moments computed for all-weather and no-rain conditions.] If the NCEP rain statistics are assumed to be roughly representative, then extratropical QuikSCAT measurements may underestimate the variance and kurtosis of the true wind stress, implying that the gridded products underestimate true wind variability even more than suggested by Fig. 5.

QuikSCAT swath data might alternatively be predicted to misrepresent true wind stresses, because unflagged rain events, instrumental noise, or retrieval algorithm shortcomings might result in more extreme events than are seen in true wind stresses. This possibility was evaluated by considering PDFs from National Data Buoy Center (NDBC) and TAO moorings in the Pacific Ocean in comparison with contemporaneous, collocated QuikSCAT wind stresses. In the Tropics, TAO wind stress means differ from swath wind stress means by more than twice the standard error in almost all cases. These differences are best explained by the fact that buoys measure absolute wind speed, while the scatterometer measures wind speed relative to the surface current (Cornillon and Park 2001; Kelly et al.

2001). Tropical variances also differ by more than twice the standard error in most cases; this too can be explained by the fact that the low-frequency variability in buoy wind stresses and scatterometer wind stresses differ because of the strong annual cycle in ocean surface currents. Otherwise, with one exception, means and variances at the NDBC buoys and skewness and kurtosis at all locations agree within 3 times the standard error. Thus, at least in regions where ocean surface currents are small, the swath wind stresses appear to provide an accurate representation of observed buoy wind stresses.

These comparisons were repeated for the five gridded data products at the NDBC buoy locations. (This analysis was not repeated for TAO buoys, because the inherent biases between in situ and scatterometer wind stresses make comparisons difficult.) None of the gridded products was as successful as the swath data at capturing the moments of PDFs computed from buoy data within three times the standard error. The COAPS, NCEP, and ECMWF products showed less disagreement than the JPL or blended wind stresses and were nearly as successful as the swath wind stresses. However, since NCEP and ECMWF analyses assimilate buoy winds (Kalnay et al. 1996; Rabier et al. 2000), the success of these products may be a result of the assimilation and does not guarantee that they provide good representations of wind stresses at locations far from in situ observations. Thus, despite the possibility of instrumental noise in the swath data, the swath wind stresses appear preferable to the gridded products for analyses that depend on knowing PDFs.

c. Temporal fluctuations of PDF moments

Since wind stresses fluctuate and undergo interannual variability, PDFs based on 4 yr of observations may not be representative of wind statistics at a particular season or moment in time. Figure 6 shows the first two moments of the stress PDFs at 55°S computed at half-month intervals starting in September 1999. Figure 7 shows the same thing at the equator. For both the zonal and meridional components, mean wind stresses fluctuate substantially from month to month, but agree within error bars for all six wind products. At 55°S, fluctuations on half-month time scales appear small compared with mean wind stresses: mean zonal wind stresses are uniformly eastward, while meridional wind stresses are almost always southward. No strong periodicity is visible in the mean wind stresses. Outside of the Southern Ocean, mean wind stresses vary with an annual periodicity that is not visible in the Southern Ocean (Fig. 6) but is clear almost everywhere to the north. The exception occurs right at the equator (Fig. 7), since winter and summer are equivalent, the annual cycle has a reduced magnitude and for the zonal winds, the semiannual cycle is more pronounced.

In contrast with the mean wind stresses, which show little periodicity at 55°S, variances for all six products have a clear annual cycle, with high variances in winter and low variances in summer. This wintertime increase in variance occurs at most latitudes and is consistent with cyclone climatologies that indicate more cyclones in winter months than in summer months (Sinclair 1994; Simmonds and Keay 2000). Similarly, Trenberth (1982) reported that compared with summer winds, winter winds had a larger variance, spread over a broader latitude range. In contrast, at the equator the variance of the meridional wind stress undergoes a semiannual cycle, with peaks near the equinoxes when the mean meridional wind changes direction. Figures 6 and 7 agree with Fig. 5 in showing that variances differ by a factor of 2 or more depending on the choice of wind product. The time series also agree with Fig. 5 in showing that swath wind stresses have the largest variances outside the Tropics, while near the equator, blended wind stresses have the largest variance. Although this analysis merges variance due to spatial variability with variance due to temporal variability, separate tests (not shown) indicate that both effects influence the seasonal cycle in variance.

The time series of skewness and kurtosis at 55°S (not shown) show little seasonality. As in Fig. 5, most of the gridded products are in rough agreement, though blended wind stresses have large kurtosis near the equator. Outside the Tropics, swath wind stresses have large skewness and kurtosis that consistently exceed the values from gridded products, implying that the gridded products do not capture the extreme events seen by the scatterometer.

4. Spectral analysis: Frequency content

Frequency spectra characterize the temporal variability of wind stress in a completely different way than PDFs. Spectra identify time scales of maximal variability but unlike PDFs provide no information about the likelihood of observing an extreme event. As with PDFs, spectra were computed for wind stress.

a. Computing frequency spectra

For this study, spectra were computed from gridded products using a fast Fourier transform (FFT) algorithm (Frigo and Johnson 1998). Of the wind products considered here, swath data require the most detailed

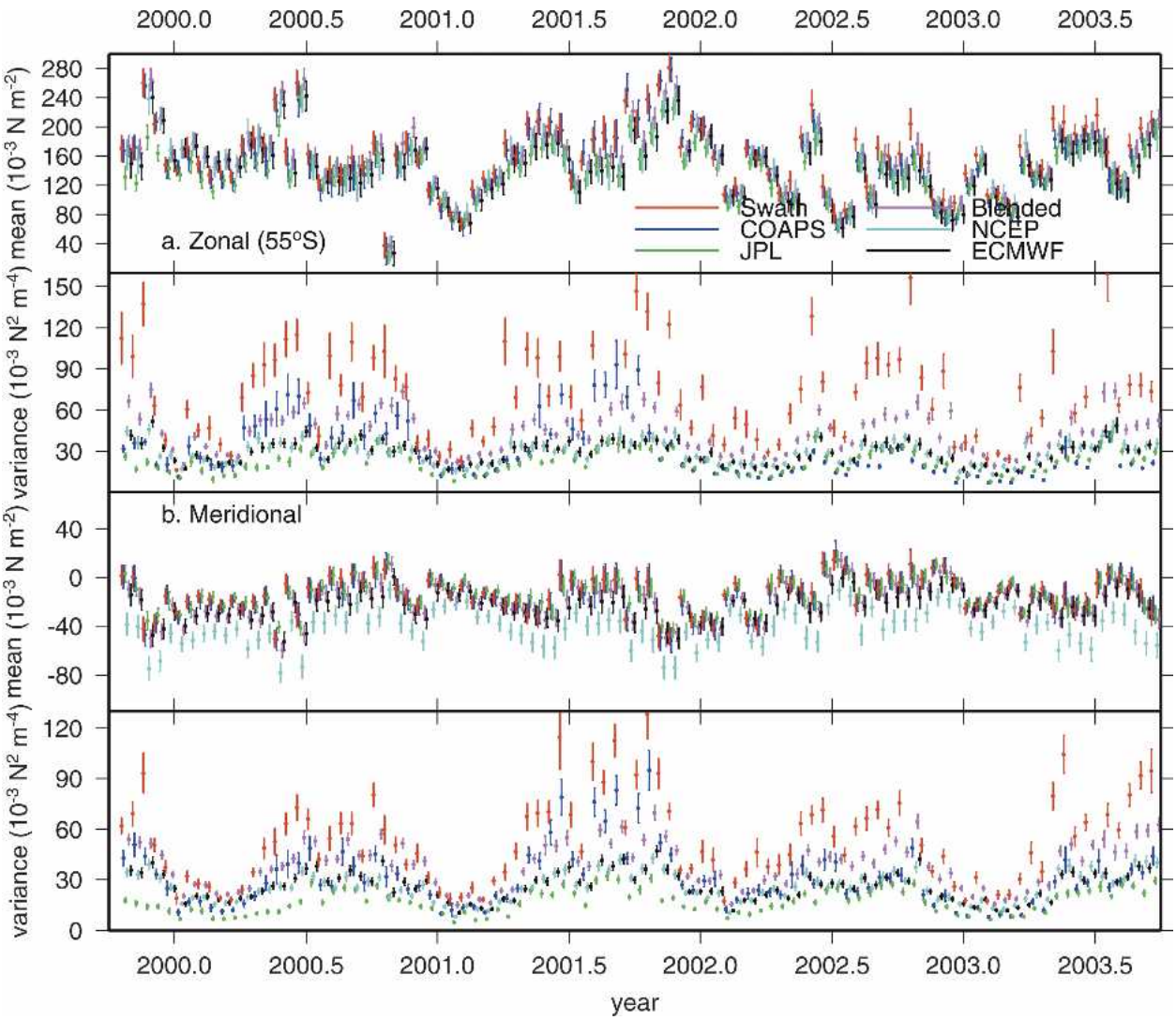

FIG. 6. First two moments (mean and variance) of (a) zonal stress PDFs and (b) meridional stress PDFs at 55°S, plotted as a function of time in half-month intervals from Sep 1999 through Aug 2003. Moments are color coded as in Fig. 5 and are offset slightly in time. Symbols may be difficult to identify when wind statistics match closely, so that one symbol overlies another.

algorithms, because they are irregularly distributed in space and time, making implementation of a standard FFT impossible. To facilitate the calculation, the data were bin averaged onto a regular spatial grid of 0.4° by 0.4°.

The scatterometer's temporal sampling posed more serious challenges. Although measurements at any given location are roughly 12 h apart in time, at about 0600 and 1800 UTC, there are numerous gaps in the data records, particularly at low to midlatitudes, where the earth's axial radius is larger and the satellite swath width is insufficient to provide twice daily coverage. A number of strategies exist to compute spectra from irregularly spaced and data full of gaps. Three were tested in this analysis. As discussed in the appendix, the results shown here are based on a simple FFT. Spectra are also computed from the five gridded wind products using an FFT. Isolated data gaps are filled with the mean of the available observations.

Swath spectra agree with spectra from the other five data products at frequencies less than about 10 cycles per year (cpy), as shown in Fig. 8. However, spectra begin to diverge at higher frequencies, where swath spectra are generally flatter than spectra from mapped fields. Spectra for the blended wind fields drop off less quickly than for other gridded fields and agree with swath spectra within statistical error bars to at least 100 cpy at all latitudes. The divergence in the gridded fields can be attributed to the fact that mapping algorithms that smooth noisy or irregular observations effectively

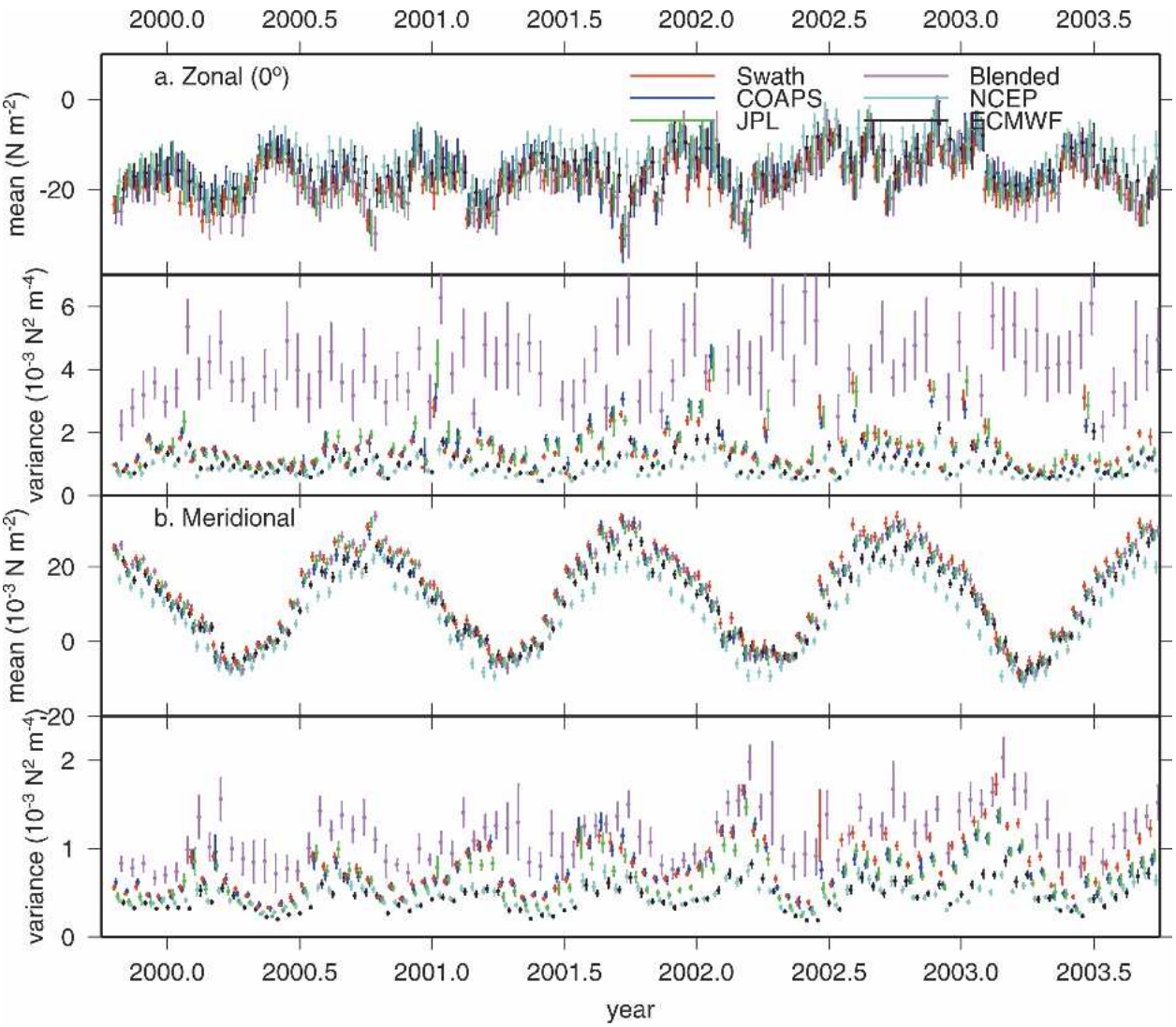

FIG. 7. First two moments (mean and variance) of (a) zonal stress PDFs and (b) meridional stress PDFs at 0° latitude, plotted as a function of time as in Fig. 6.

apply a low-pass filter, thus attenuating high-frequency variability.

Here swath spectra are presented in detail as a function of latitude. Figure 9 shows spectra for the zonal stress of swath winds at 5° latitude increments, and Fig. 10 shows the same thing for meridional stress. For these calculations, spectra are computed at each available location in longitude and are averaged zonally. The number of degrees of freedom is determined by scaling the number of longitude points N by the zonal and meridional decorrelation scales derived for μ_1 in Table 1. Error bars in these figures are formally constant for all frequencies and are larger in the Northern Hemisphere, because the Northern Hemisphere contains less ocean than the Southern Hemisphere. Zonal wind stress spectra have larger error bars than meridional spectra, because meridional winds decorrelate more rapidly than zonal winds with longitude, and therefore are assumed to have more degrees of freedom.

Comparisons of the first and second columns of Figs. 9 and 10 indicate that Northern and Southern Hemisphere spectra vary with latitude in similar ways, with a few exceptions. At all latitudes there are spectral peaks corresponding to annual and semiannual variability. As discussed in the appendix, high-frequency spectral peaks at low latitudes are an artifact of sampling gaps in the scatterometer winds. In the Southern Ocean, poleward from 50°S, the annual peak is not statistically distinguishable from the semiannual peak. Poleward from 50°N, in the Northern Hemisphere, error bars are

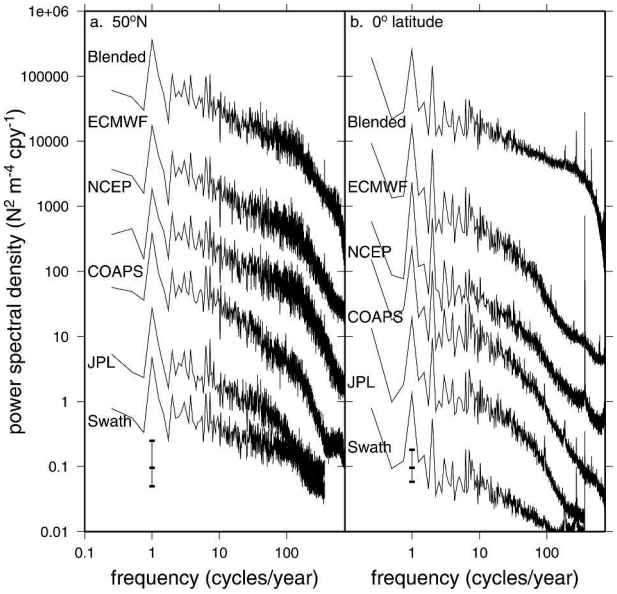

FIG. 8. Spectra computed for wind stress from all six zonal products at (a) 50°N and (b) at 0°. These latitudes were selected to roughly coincide with buoy locations. Note that spectral power differs by a factor of 10 at 50°N compared with the equator. Spectra are offset by powers of 10 to separate the different plots.

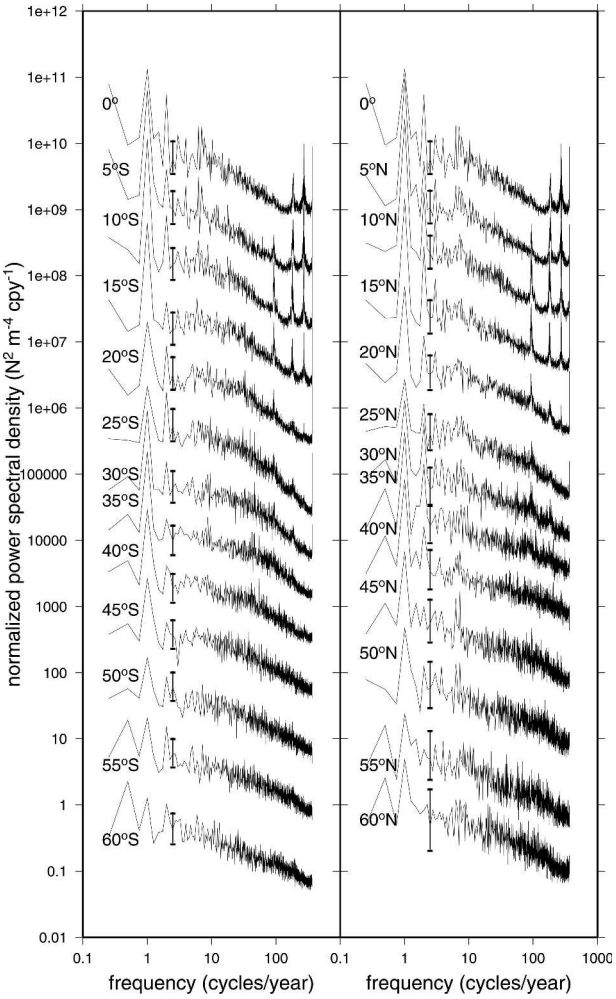

FIG. 9. Frequency spectra for zonal stress at 5° latitude intervals from (left) 0° to 60°S and (right) 0° to 60°N, scaled by powers of 10. Spectra are computed using an FFT for 4 yr of swath scatterometer wind observations and then zonally averaged for all ocean locations. Normalization and error bars are as in Fig. 13. Equatorial spectra are plotted twice for symmetry.

large, and while the semiannual cycle is less energetic, the annual cycle itself is not statistically distinguishable from other low-frequency variability. Meridional wind stresses show strong variability on the annual and semiannual cycles, with the annual cycle peak exceeding the semiannual peak at all latitudes. The meridional component indicates more low frequency spectral power in the high-latitude Northern Hemisphere than in the high-latitude Southern Hemisphere: the annual cycle at 60°N is 7.3 times more energetic than the annual cycle at 60°S, a difference that exceeds the error bars.

Are the swath spectra representative of "true" wind stress spectra? The scatterometer's 12-h sampling pattern does not record high-frequency fluctuations of the wind, and this can have a significant impact on spectra. Figure 11 shows spectra from the TAO and NDBC buoys. Spectra are computed from hourly observations (black lines) and from buoy records subsampled at 12-h intervals to resemble scatterometer sampling (gray lines). Because of aliasing effects, the spectra diverge for frequencies greater than about 100 cpy. These plots indicate that above 100 cpy, spectral slopes determined from scatterometry (or any other wind product sampled at 12-h intervals) are likely to be flat relative to true spectra. Similar aliasing patterns have been reported for other types of satellite data (e.g., Tierney et al. 2000; Stammer et al. 2000). Thus the discussion that follows will distinguish between lower frequencies where aliasing is unlikely to bias the results, and higher frequencies where aliasing may substantially influence the interpretation.

b. *Spectral slopes*

Spectral slopes are used here to examine the frequency content of the wind stress driving the ocean. Spectra computed from wind velocities are not shown here but are steeper by a factor of about $\omega^{0.1}$ than pseudostress spectra, which in turn are steeper than wind stress spectra by about $\omega^{0.1}$. Nonetheless, as a simple first guess, if the mean flow were strong compared with fluctuations, then one might suppose that frequency

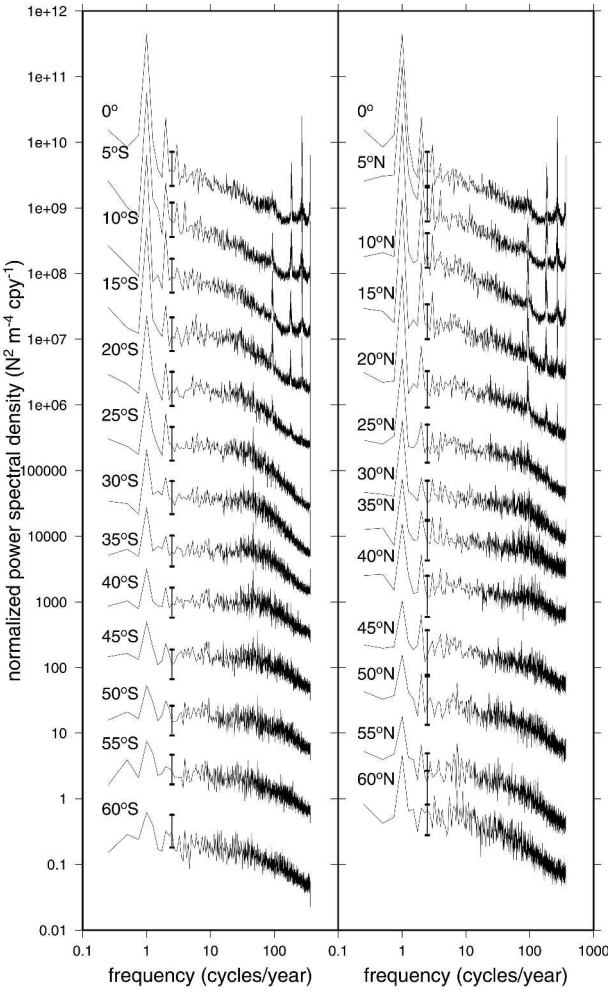

FIG. 10. Frequency spectra for meridional stress at 5° latitude intervals, as in Fig. 9.

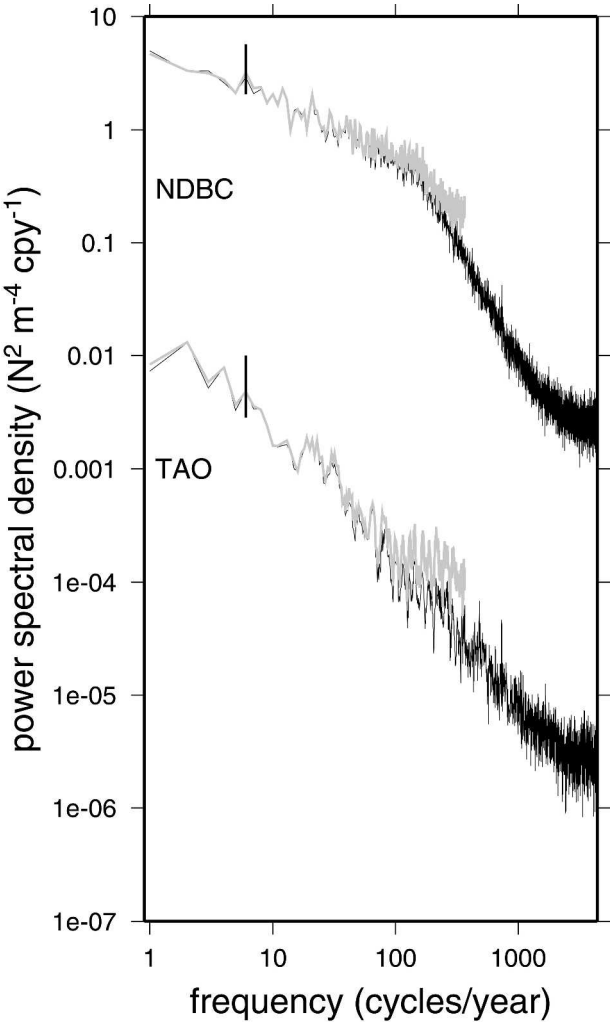

FIG. 11. Spectra computed from TAO and NDBC buoys based on hourly data (black lines) and data subsampled at 12-h intervals to resemble twice daily scatterometer sampling (gray lines). NDBC spectra are multiplied by 10. Spectra are computed for one year periods of data. For NDBC, 35 time series are used, for which no more than 15% of data are missing; for TAO, 42 time series are used, for which no more than 25% of data are missing. Normalization is the same as in other spectra. Gray and black lines diverge for frequencies greater than about 100 cpy, indicating that scatterometer sampling is likely to alias high-frequency variability.

spectra should resemble wavenumber spectra (e.g., Taylor 1938; Frisch 1995), which for velocities have been shown to decay like $k^{-5/3}$ in the Tropics (Wikle et al. 1999) and like k^{-2} in the extratropics (Freilich and Chelton 1986; Chin et al. 1998), in rough agreement with the predictions of turbulence theory (Nastrom and Gage 1985; Frisch 1995). However, the Taylor hypothesis is not expected to apply for the time scales resolved by the scatterometer (Powell and Elderkin 1974), and the wind stress spectra found here are considerably flatter than wavenumber spectra.

Figure 12 plots best estimates of spectral slopes in two frequency bands for the five gridded products as well as swath wind stresses and buoy data. Spectral slopes vary substantially with latitude and differ by a factor of 2 or more depending on wind product. In the frequency band between 10 and 90 cpy, spectra for swath data decay like $\omega^{-1/2}$ for zonal stress and like $\omega^{-1/3}$ for meridional stress, substantially flatter than idealized turbulence theory would predict. All five gridded wind products have steeper spectral slopes, at all latitudes, with the exception of the blended winds in the Tropics. This may be partly due to residual noise in the swath data, although the spectra would be expected to be flat if the data were contaminated with true white noise. In addition, as noted by Yang and Shapiro (1973), interpolation algorithms, such as those used to

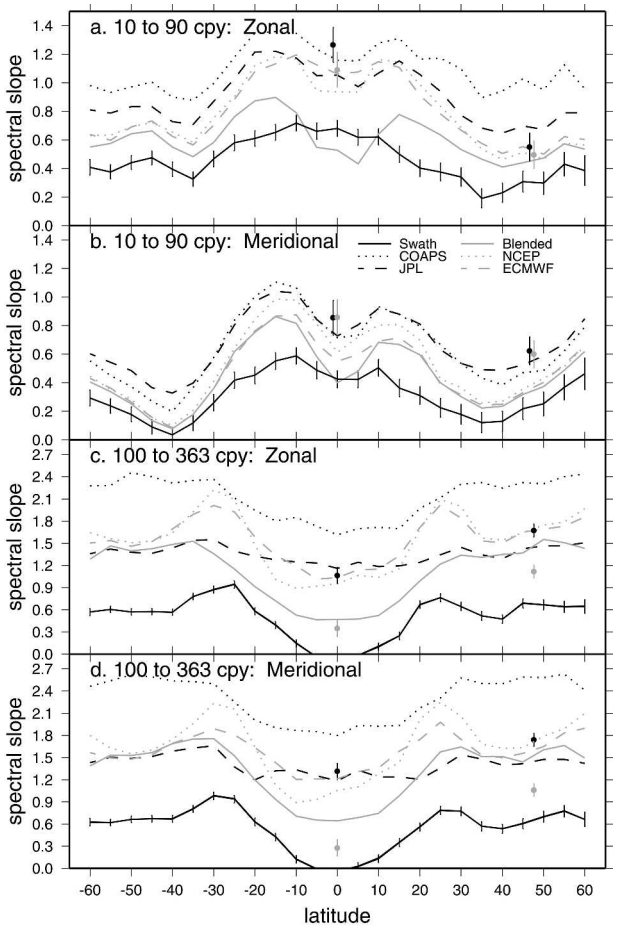

FIG. 12. (a) Negative of spectral slopes for zonal stress as a function of latitude in the frequency band between 10 and 90 cpy for six wind products [lines, legend in (b)] and for TAO and NDBC buoys (dots). Buoy data slopes in black are computed using hourly measurements; points in gray are computed from spectra determined using 12-h subsamples. Black points are offset by 1° to ensure that all measurements are visible. (b) Same thing for meridional wind stresses. (c) Same for zonal stress in the frequency band between 100 and 363 cpy. Swath slopes equatorward of 30° latitude are considered unreliable, because peaks associated with sampling gaps are likely to bias the slope estimates. (d) Same as (c) for meridional wind stresses. In all cases, slopes are determined from the spectra in Figs. 9 and 10 (and from equivalent spectra computed using the other wind products) using a least squares fitting procedure. Error bars are shown for swath spectra only but are comparable for other data products, since each provides similar numbers of statistically independent wind measurements at each latitude. Error bars represent 95% confidence limits and are determined from the least squares fitting procedure.

grid wind observations, can artificially steepen spectral slopes.

The five gridded wind products have spectral slopes that vary in latitude in much the same way as the swath spectra. In general, the meridional component of the wind has flatter slopes and more closely resembles white noise than the zonal component. For both wind components, spectral slopes are steepest around 15° latitude and at high latitudes. The latitudes of steepest spectral slope coincide with latitudes in Fig. 5 where mean wind stresses reach maxima. Spectral slopes are flattest at the equator and around 40° latitude; these places coincide with latitudes where the mean wind stresses are near zero. Variations in slope thus appear linked to the large-scale meridional circulation of the atmosphere: spectral slopes increase as the mean wind speed increases, because strong mean wind stresses coincide with strong low-frequency wind variability.

In the higher frequency band between 100 and 363 cpy, slopes are slightly steeper, averaging from about 0.6 for swath wind stresses outside the Tropics up to about 2.7 for COAPS wind stresses at high latitudes. The range of slopes is substantial, and none of the gridded products consistently agrees with the swath spectral slopes. However, swath wind slopes are suspect in the Tropics, because spikes associated with data gaps distort the slope calculation. (Resonant spectral peaks at high frequencies may also bias the spectral slopes for other data products.) Swath and gridded wind products agree in showing that spectral slopes in this frequency range are at a minimum at the equator and are steepest near 30° latitude. In general, in the 100–363-cpy range, meridional slopes slightly exceed zonal slopes, though the slopes are essentially the same within error bars.

Buoy wind stresses offer an independent measure of the wind spectra. In Fig. 12, gray dots indicate spectral slopes computed from buoy data subsampled at 12-h intervals, and black dots indicate spectral slopes from hourly buoy data. In the 10–90-cpy-frequency range, gray and black dots are the same within error bars, but in the 100–363-cpy frequency range they differ significantly. Since the data products shown here are reported at 6- or 12-h intervals, they are expected to agree more closely with the gray dots than the black dots. The buoy wind stresses do not show a systematic pattern of agreement with gridded products. In the 10–90-cpy frequency band, the zonal component of the midlatitude NDBC wind stress spectral slopes most closely matches the blended, NCEP, and ECMWF spectral slopes, while the TAO zonal component best agrees with COAPS, JPL, and ECMWF spectral slopes. For both latitude ranges, the spectral slope of the meridional wind stress component is relatively steep and best agrees with COAPS or JPL wind stresses. In the 100–363-cpy frequency range, the gray dots fall in between the blended and swath spectral slopes for all cases.

However, the buoy comparisons may be question-

able for a number of reasons. Differences between scatterometer and buoy spectra in the tropical region are not explained by differences between no-rain and all-weather TAO measurements but can be explained by a number of other factors. First, since buoys measure wind relative to geographic coordinates, while scatterometry measures wind relative to upper ocean currents, the scatterometer measurements do not include low-frequency fluctuations in surface currents that dominate tropical ocean variability. This means that scatterometer spectra are less energetic at low frequencies and therefore have flatter spectral slopes. In addition, buoy and scatterometer spectra also differ for reasons that have more to do with temporal sampling patterns rather than the physics of the wind. Buoys do not always return complete 12-month intervals of wind data. Here in order to facilitate simple comparisons, buoy data gaps (due to temporary or permanent instrument failures) were filled with the mean of available observations. TAO data were used only if at least 75% of available time slots had observations and NDBC data only if at least 85% of available time slots had observations. This sampling pattern differs substantially from scatterometer sampling, which provides relatively uniform (though gappy) sampling through the year, and these differences are likely to result in decreased spectral power at high-frequency and therefore steeper spectral slopes. Finally, in order to reduce the spectral error bars for this analysis, buoy and scatterometer data were mismatched in time and space. Buoy data were localized in small geographic regions, but represented all years from 1990 onward in which adequate observations were collected. In contrast scatterometer wind spectra were computed using just four years of available data, averaged over all longitudes. A more careful match in space and time would have reduced the number of degrees of freedom so that the spectral slopes were indistinguishable from zero. While dominant ocean variability patterns depend on latitude, spectral structures also vary with longitude (not shown). Regions with less storm activity, such as the eastern tropical Pacific, have lower variance and kurtosis and flatter spectral slopes than stormier regions.

In contrast to the comparatively flat slopes observed in these wind stress spectra, ocean velocities have somewhat steeper spectra, usually reported around ω^{-2} for Eulerian velocities (Wunsch 1981) or ω^{-3} for Lagrangian velocities (Rupolo et al. 1996). This difference between wind stress and ocean velocity spectra implies that the ocean does not directly mirror wind forcing, but instead responds to the cumulative effect of long-term fluctuations in wind forcing, as has been reported elsewhere (e.g., Sura and Gille 2003).

5. Summary

This study has examined statistical properties of swath scatterometer wind stresses in comparison with five different global gridded wind stress fields as well as wind stress data from selected buoys in the Pacific Ocean. The statistics used in this study, PDFs and frequency spectra, provide distinct characterizations of the wind that drives ocean circulation.

PDFs show that wind stress components have non-Gaussian distributions and that these distributions evolve in time, generally showing higher variances in winter than summer. If swath data are taken as a benchmark, then clearly none of the gridded products measures up to their standard. Scatterometer swath wind stresses indicate strong variability with large numbers of extreme events. Variances differ by as much as a factor of 2 for different wind products, with highest variances in swath and blended wind stresses. Gridded products fail to capture the true variance of the data, much less the subtleties of skewness and kurtosis. Although the swath wind stresses may suffer from instrumental or retrieval errors, PDFs computed from swath wind stresses agree within error bars with PDFs computed from North Pacific buoy wind observations. If anything, swath wind stresses might be expected to underestimate extreme events, since extreme wind stresses that occur during heavy rains are discarded from the scatterometer records, resulting in the rejection of a large fraction of measurements from events such as hurricanes.

Frequency spectra are red, but the spectral slopes are small, implying that wind fields vary substantially over a broad range of frequencies. This energetic high-frequency variability is difficult to capture from the two measurements per day available from QuikSCAT, but might be better represented from a tandem mission of SeaWinds instruments. NASA has no current plans for a tandem mission, following the early failure of the *Midori-II* satellite, which carried a second SeaWinds scatterometer that operated from April through October 2003. The European Space Agency will have scatterometers of a slightly different design on their MetOp satellites, the first of which is scheduled to launch in 2006.

Wind spectra largely agree for the six products at frequencies less than about 10 cycles per year. At higher frequencies, latitudinal variations of spectral slopes follow similar patterns for all wind products considered, but the actual slope values differ considerably, and swath spectra are systematically flatter than spectra derived from gridded wind stresses. Swath spectra also appear flat relative to buoy wind stresses. However,

buoys offer an imperfect ground truth for scatterometer measurements, because they measure wind stresses relative to a fixed geographic point, while the scatterometer measures wind stresses relative to the mean ocean currents. In the frequency band between 10 and 90 cpy, where the scatterometer spectral slopes are expected to be reasonable, none of the gridded products match the swath wind stresses at all latitudes. Gridding procedures can artificially steepen spectral slopes (Yang and Shapiro 1973). Thus differences in mapping algorithms may account for the wide range of spectral slopes observed in these data.

Together these findings suggest that gridded wind products do a good job of reproducing some characteristics of the swath wind stresses, such as mean wind fields and basic latitudinal trends that indicate greater variance at high latitudes and high spectral slopes near the equator in the 10–90-cpy frequency band. However, none of the gridded products fully captures the variance, the frequency of extreme events, or the frequency spectra seen by the scatterometer. Gridded wind products should be selected with these issues in mind. Scatterometer swath wind stresses have a number of potential problems: they reject data collected under rainy conditions, they report occasional erroneous extreme wind events associated with unflagged rain events, they do not smooth out random errors, and they have regular spaced sampling gaps. If these caveats are judged to be minor limitations and the scatterometer swath data are assumed to be correct, then the results of this study suggest that where possible, swath wind stresses should be used rather than gridded products to characterize the wind stresses that drive the ocean.

Acknowledgments. Marina Gurary carried out much of the programming required to make this analysis possible. QuikSCAT data are processed by Remote Sensing Systems with sponsorship from the NASA Ocean Vector Winds Science Team. The Compact Level 2B product used for this study is produced and distributed by COAPS at Florida State University, based on the Ku2001 algorithm winds developed by Remote Sensing Systems. COAPS gridded winds and advice about using them were provided by Mark Bourassa (available online at http://www.coaps.fsu.edu). JPL winds came from Tim Liu and Wendy Tang (available online at http://airsea-www.jpl.nasa.gov/seaflux). Blended winds were provided by Ralph Milliff and Jan Morzel of Colorado Research Associates (available online at http://dss.ucar.edu/datasets/ds744.4/). ECMWF winds were obtained from the National Center for Atmospheric Research, Boulder, Colorado. Joey Comeaux provided helpful advice about reading the wind fields. NCEP Reanalysis data provided by the NOAA–CIRES Climate Diagnostics Center, Boulder, Colorado; (from their Web site at http://www.cdc.noaa.gov/; NDBC buoy data were downloaded from http://www.ndbc.noaa.gov/). TAO data were provided by the TAO Project Office (http://www.pmel.noaa.gov/tao/jsdisplay/). Additional useful comments came from Mark Bourassa, Mike Freilich, Kathie Kelly, Stefan Llewellyn Smith, and the anonymous reviewers. This research was supported by the NASA Ocean Vector Wind Science Team, JPL Contract 1222984.

APPENDIX

Spectral Methods for Gappy Scatterometer Observations

Three basic strategies were tested for computing spectra from scatterometer observations. The most straightforward strategy is to treat the data as if they are regularly spaced in time at 12-h intervals. Data gaps are replaced with the mean wind value at the same location. This allows a fast Fourier transform (FFT) to be applied and spectra to be computed. In Fig. A1, spectra based on FFTs are second from the top.

Spectra computed from data can sometimes be bi-

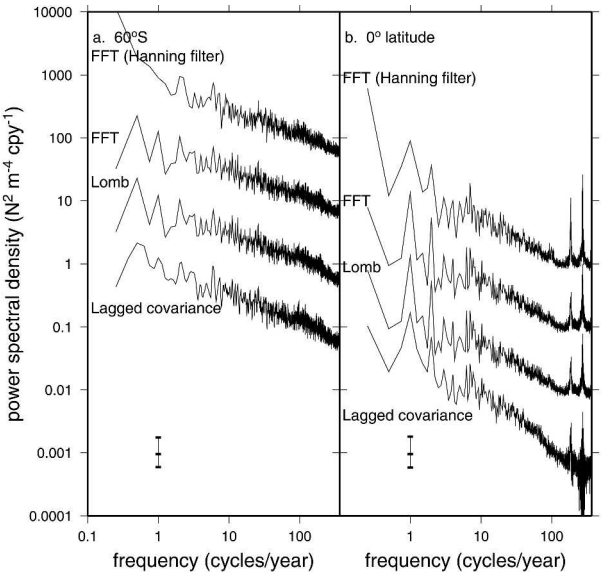

FIG. A1. Frequency spectra computed using the FFT, FFT with Hanning filter, Lomb–Scargle, and lagged covariance methods for zonal stress at (left) 60°S and (right) at the equator. Error bars represent 95% confidence limits. Since wind data are spatially correlated, the number of degrees of freedom is equal to the number of locations for which measurements are obtained at each latitude, adjusted by the decorrelation length scale. From bottom to top, spectra are scaled by factors of 1, 10, 100, and 1000, respectively. Spectra are normalized so that $\Sigma_{i=1}^{N}\tau_i^2 = \Sigma_{j=1}^{N/2}s_j$, where τ_i represent stress estimates at half-day intervals and s_j represent spectra at frequency increments of 1 cycle per 4 yr.

ased by sidelobes (or spectral ringing) associated with the finite duration of the time series. Percival and Walden (1993) provide a careful discussion of the topic and suggest either tapering or prewhitening the observations before computing spectra. Prewhitening is most appropriate for data with a large dynamic range or well-known spectral characteristics, neither of which applies in this case. A Hanning filter has been tested to taper the data (topmost spectra in Fig. A1). The Hanning filter shifts spectral power between the time constant and lowest frequency variations, and tests with idealized red noise indicate that this can bias the lowest frequency estimates of spectral slope. For the scatterometer data, the Hanning filter has little impact on high-frequency spectral slopes. Thus, in this analysis, a Hanning filter is not routinely applied and spectral slopes are assumed not to be significantly biased by the finite duration of the data records.

Since satellite winds are measured within a swath, the local time of measurement can vary by an hour or more depending on the latitude. Thus, the assumption that winds are regularly spaced at 12-h intervals may introduce errors into the spectra. The Lomb normalized periodogram (Press and Rybicki 1989) is designed to carry out fast computation of spectra even in cases in which data are irregularly spaced and gappy. The method, summarized by Press et al. (1992), was designed largely for identifying significant spectral peaks in astrophysical data, rather than examining spectral slopes in turbulent geophysical flows. The fast Lomb algorithm "extirpolates" irregular data onto a regular grid so that an FFT can be performed. While the method described by Press et al. (1992) defines the regular grid based on the average interval between observations, for this study the algorithm was modified to predefine the temporal spacing of the extirpolated points, so that multiple spectra could be averaged together. The fast Lomb algorithm closely resembles an FFT: in cases where data are regularly spaced but gappy, spectra computed using this algorithm are expected to be the same as spectra computed using the FFT described above. In Fig. A1 there is little difference between the second and third spectra, indicating that the Lomb algorithm's corrections for exact time of sampling are not critical for these scatterometer winds.

Scatterometer data can have gaps due to instrument failure or rain conditions, but most gaps occur because the satellite orbit misses parts of the earth each day. Thus gaps tend to occur at regular time intervals, depending on latitude. Schlax et al. (2001) provided a comprehensive analysis of the impact of this sampling on mapped wind fields. Here we consider the impact of the sampling gaps on spectra. Because the FFT implementation used here and the Lomb algorithm both fill all gaps with the same data value, this can result in an apparent spectral peak associated with the gap interval. In Fig. A1 spectral peaks associated with temporal sampling gaps are evident at frequencies of 1 cycle every 2 days (185 cpy) and 3 cycles every 4 days (243 cpy). Similar alias patterns occur in all spectra equatorward of about 35° latitude. Between 5° and 20° latitude a peak is also visible at 1 cycle every 4 days (93 cpy). A strategy for minimizing the impact of gaps is to compute the Fourier transform of the lagged covariance. Provided that the covariance at zero lag exceeds all other covariances and that at least some observations are collected for all possible time intervals so that the lagged covariance is gap free, then spectra can be derived that in principle should not depend strongly on the sampling increments. For swath winds, the lagged covariance is computed for time separations incremented at half-day intervals. In the resulting spectra (bottom of Fig. A1), spectral peaks associated with the data gaps are reduced. Instead the spectra indicate substantial point-to-point variations near the alias frequency. These fluctuations in spectral power can be slightly reduced by filtering the spectra, but they are not easily removed entirely.

Overall, the spectra plotted in Fig. A1 agree within error bars regardless of method, except at the frequencies associated with data sampling gaps. Because of the sampling problems at high frequencies, at low latitudes spectra based on QuikSCAT swath winds are probably best interpreted for frequencies lower than 90 cpy. Better sampling through a tandem satellite mission would be required to resolve 1–4-day variability that might be associated with propagating frontal systems or other storm track variability. Because the three spectral methods discussed here are very similar, results presented in the main body of this paper focus on findings from the simple FFT.

REFERENCES

Bauer, E., 1996: Characteristic frequency distributions of remotely sensed in situ and modelled wind speeds. *Int. J. Climatol.,* **16,** 1089–1102.

Bourassa, M. A., 2004: An improved sea state dependency for surface stress derived from in situ and remotely sensed winds. *Adv. Space Res.,* **33,** 1136–1142.

——, D. M. Legler, J. J. O'Brien, and S. R. Smith, 2003: SeaWinds validation with research vessels. *J. Geophys. Res.,* **108,** 3019, doi: 10.1029/2001JC001028.

Chen, D., W. T. Liu, S. E. Zebiak, M. A. Cane, Y. Kushnir, and D. Witter, 1999: Sensitivity of the tropical Pacific Ocean to the temporal and spatial resolution of wind forcing. *J. Geophys. Res.,* **104,** 11 261–11 271.

Chin, T. M., R. F. Milliff, and W. G. Large, 1998: Basin-scale high-

wavenumber sea surface wind fields from multiresolution analysis of scatterometer data. *J. Atmos. Oceanic Technol.,* **15,** 741–763.

Cornillon, P., and K.-A. Park, 2001: Warm core ring velocities inferred from NSCAT. *Geophys. Res. Lett.,* **28,** 575–578.

Davis, R. E., 1976: Predictability of sea surface temperature and sea level pressure anomalies over the North Pacific Ocean. *J. Phys. Oceanogr.,* **6,** 249–266.

Ebuchi, N., 1999: Statistical distribution of wind speeds and directions globally observed by NSCAT. *J. Geophys. Res.,* **104,** 11 393–11 403.

Elipot, S., and S. Gille, 2002: Spectral response of the Southern Ocean surface circulation to wind. *Proc. WOCE and Beyond,* San Antonio, TX, NOAA.

Freilich, M. H., and D. B. Chelton, 1986: Wavenumber spectra of Pacific winds measured by the Seasat scatterometer. *J. Phys. Oceanogr.,* **16,** 741–757.

——, and P. G. Challenor, 1994: A new approach for determining fully empirical altimeter wind speed model functions. *J. Geophys. Res.,* **99,** 25 051–25 062.

——, and R. S. Dunbar, 1999: The accuracy of the NSCAT 1 vector winds: Comparisons with National Data Buoy Center buoys. *J. Geophys. Res.,* **104,** 11 231–11 246.

Frigo, M., and S. G. Johnson, 1998: FFTW: An adaptive software architecture for the FFT. *Proc. Int. Conf. on Acoustics, Speech, and Signal Processing,* Seattle, WA, ICASSP, 1381–1384.

Frisch, U., 1995: *Turbulence.* Cambridge University Press, 296 pp.

Gille, S. T., and S. G. Llewellyn Smith, 2000: Velocity-variance probability distribution functions from altimeter measurements. *J. Phys. Oceanogr.,* **30,** 125–136.

——, D. P. Stevens, R. T. Tokmakian, and K. J. Heywood, 2001: Antarctic Circumpolar Current response to zonally-averaged winds. *J. Geophys. Res.,* **106,** 2743–2759.

Hersbach, H., L. Isaksen, and P. A. E. M. Janssen, 2003: Operational assimilation of QuikSCAT data at ECMWF. Preprints, *12th Conf. on Satellite Meteorology and Oceanography,* Long Beach, CA, Amer. Meteor. Soc., CD-ROM, 5.1.

Kalnay, E., and Coauthors, 1996: The NCEP–NCAR 40-Year Reanalysis Project. *Bull. Amer. Meteor. Soc.,* **77,** 437–471.

Kelly, K. A., S. Dickinson, M. J. McPhaden, and G. C. Johnson, 2001: Ocean currents evident in satellite wind data. *Geophys. Res. Lett.,* **28,** 2469–2472.

Kistler, R., and Coauthors, 2001: The NCEP–NCAR 50-year reanalysis: Monthly means CD-ROM and documentation. *Bull. Amer. Meteor. Soc.,* **82,** 247–267.

Kraus, E. B., and J. S. Turner, 1967: A one-dimensional model of the seasonal thermocline: II. The general theory and its consequences. *Tellus,* **19,** 98–106.

Levy, G., 1994: Southern Hemisphere low level wind circulation statistics from the Seasat scatterometer. *Ann. Geophys.,* **12,** 65–79.

Liu, W. T., and W. Tang, 1996: Equivalent neutral wind. JPL Publication 96–17, Jet Propulsion Laboratory, Pasadena, CA, 8 pp. [Available online at http://airsea-www.jpl.nasa.gov/publication/lkb.html.]

——, K. B. Katsaros, and J. A. Businger, 1979: Bulk parameterization of air-sea exchanges of heat and water vapor including the molecular constraints at the interface. *J. Atmos. Sci.,* **36,** 1722–1735.

——, W. Q. Tang, and P. S. Polito, 1998: NASA scatterometer provides global ocean-surface wind fields with more structures than numerical weather prediction. *Geophys. Res. Lett.,* **25,** 761–764.

Lungu, T., 2001: QuikSCAT Science Data Product User's Manual, Version 2.2 D-18053, Jet Propulsion Laboratory, 95 pp.

Mestas-Nuñez, A. M., D. B. Chelton, M. H. Freilich, and J. G. Richman, 1994: An evaluation of ECMWF-based climatological wind stress fields. *J. Phys. Oceanogr.,* **24,** 1532–1549.

Milliff, R. F., W. G. Large, W. R. Holland, and J. C. McWilliams, 1996: The general circulation responses of high-resolution North Atlantic Ocean models to synthetic scatterometer winds. *J. Phys. Oceanogr.,* **26,** 1747–1768.

——, ——, J. Morzel, G. Danabasoglu, and T. M. Chin, 1999: Ocean general circulation model sensitivity to forcing from scatterometer winds. *J. Geophys. Res.,* **104,** 11 337–11 358.

——, J. Morzel, D. B. Chelton, and M. H. Freilich, 2004: Wind stress curl and wind stress divergence biases from rain effects on QSCAT surface wind retrievals. *J. Atmos. Oceanic Technol.,* **21,** 1216–1231.

Monahan, A. H., 2004a: Low-frequency variability of the statistical moments of sea-surface winds. *Geophys. Res. Lett.,* **31,** L10302, doi: 10.1029/2004GL019599.

——, 2004b: A simple model for the skewness of global sea-surface winds. *J. Atmos. Sci.,* **61,** 2037–2049.

Nastrom, G. D., and K. S. Gage, 1985: A climatology of atmospheric wavenumber spectra of wind and temperature observed by commercial aircraft. *J. Atmos. Sci.,* **42,** 950–960.

Pegion, P. J., M. A. Bourassa, D. M. Legler, and J. J. O'Brien, 2000: Objective derived daily "winds" from satellite scatterometer data. *Mon. Wea. Rev.,* **128,** 3150–3168.

Percival, D. B., and A. T. Walden, 1993: *Spectral Analysis for Physical Applications.* Cambridge University Press, 583 pp.

Pickett, M. H., W. Tang, L. K. Rosenfeld, and C. H. Wash, 2003: QuikSCAT satellite comparisons with near-shore buoy wind data off the U.S. West Coast. Preprints, *12th Conf. on Satellite Meteorology and Oceanography,* Long Beach, CA, Amer. Meteor. Soc., CD-ROM, JP4.2.

Powell, D. C., and C. E. Elderkin, 1974: An investigation of the application of Taylor's hypothesis to atmospheric boundary layer turbulence. *J. Atmos. Sci.,* **31,** 990–1002.

Powell, M. D., P. J. Vickery, and T. A. Reinhold, 2003: Reduced drag coefficient for high wind speeds in tropical cyclones. *Nature,* **422,** 279–283.

Press, W. H., and G. B. Rybicki, 1989: Fast algorithm for spectral analysis of unevenly sampled data. *Astrophys. J.,* **338,** 277–280.

——, B. P. Flannery, S. A. Teukolsky, and W. T. Vetterling, 1992: *Numerical Recipes in C: The Art of Scientific Computing.* Cambridge University Press, 994 pp.

QuikSCAT Project, 2000: QuikSCAT Project Data Release Notes. Tech. Rep., Jet Propulsion Laboratory, California Institute of Technology, 6 pp.

Quilfen, Y., B. Chapron, and D. Vandemark, 2001: The ERS scatterometer wind measurement accuracy: Evidence of seasonal and regional biases. *J. Atmos. Oceanic Technol.,* **18,** 1684–1697.

Rabier, F., H. Järvinen, E. Klinker, J. F. Mahfouf, and A. Simmons, 2000: The ECMWF operational implementation of four-dimensional variational assimilation. I: Experimental results with simplified physics. *Quart. J. Roy. Meteor. Soc.,* **126,** 1143–1170.

Rupolo, V., B. L. Hua, A. Provenzale, and V. Artale, 1996:

Lagrangian velocity spectra at 700 m in the western North Atlantic. *J. Phys. Oceanogr.,* **26,** 1591–1607.

Schlax, M. G., D. B. Chelton, and M. H. Freilich, 2001: Sampling errors in wind fields constructed from single and tandem scatterometer datasets. *J. Atmos. Oceanic Technol.,* **18,** 1014–1036.

Simmonds, I., and K. Keay, 2000: Mean Southern Hemisphere extratropical cyclone behavior in the 40-year NCEP–NCAR reanalysis. *J. Climate,* **13,** 873–885.

Sinclair, M. R., 1994: An objective cyclone climatology for the Southern Hemisphere. *Mon. Wea. Rev.,* **122,** 2239–2256.

Stammer, D., C. Wunsch, and R. M. Ponte, 2000: De-aliasing of global high frequency barotropic motions in altimeter observations. *Geophys. Res. Lett.,* **27,** 1175–1178.

Sura, P., 2003: Stochastic analysis of Southern and Pacific Ocean sea surface winds. *J. Atmos. Sci.,* **60,** 654–666.

——, and C. Penland, 2002: Sensitivity of a double-gyre model to details of stochastic forcing. *Ocean Modelling,* **4,** 327–345.

——, and S. T. Gille, 2003: Interpreting wind-driven Southern Ocean variability in a stochastic framework. *J. Mar. Res.,* **61,** 313–334.

Tang, W., and W. T. Liu, 1996: Objective interpolation of scatterometer winds. JPL Tech. Rep. 96-19, 16 pp.

Taylor, G. I., 1938: The spectrum of turbulence. *Proc. Roy. Soc. London,* **A165,** 476–484.

Tierney, C., J. Wahr, F. Bryan, and V. Zlotnicki, 2000: Short-period oceanic circulation: Implications for satellite altimetry. *Geophys. Res. Lett.,* **27,** 1255–1258.

Trenberth, K. E., 1982: Seasonality in Southern Hemisphere eddy statistics at 500 mb. *J. Atmos. Sci.,* **39,** 2507–2520.

Wanninkhof, R., 1992: Relationship between wind speed and gas exchange over the ocean. *J. Geophys. Res.,* **97,** 7373–7382.

——, and W. R. McGillis, 1999: A cubic relationship between air-sea CO_2 exchange and wind speed. *Geophys. Res. Lett.,* **26,** 1889–1892.

Weijer, W., 2005: High-frequency wind forcing of a channel model of the ACC: Normal mode excitation. *Ocean Modelling,* **9,** 31–50.

Wentz, F., D. K. Smith, C. A. Mears, and C. L. Gentemann, 2001: Advanced algorithms for QuikScat and SeaWinds/AMSR. *Proc. Int. Geoscience and Remote Sensing Symp.,* Sydney, Australia, IEEE, 1079–1081.

Wikle, C. K., R. F. Milliff, and W. G. Large, 1999: Surface wind variability on spatial scales from 1 to 1000 km observed during TOGA COARE. *J. Atmos. Sci.,* **56,** 2222–2231.

Wunsch, C., 1981: Low-frequency variability of the sea. *Evolution of Physical Oceanography,* B. A. Warren and C. Wunsch, Eds., MIT Press, 342–374.

Yang, C. H., and R. Shapiro, 1973: The effects of the observational system and the method of interpolation on the computation of spectra. *J. Atmos. Sci.,* **30,** 530–536.

Yelland, M., and P. K. Taylor, 1996: Wind stress measurements from the open ocean. *J. Phys. Oceanogr.,* **26,** 541–558.

——, B. I. Moat, P. K. Taylor, R. W. Pascal, J. Hutchings, and V. C. Cornell, 1998: Wind stress measurements from the open ocean corrected for airflow distortion by the ship. *J. Phys. Oceanogr.,* **28,** 1511–1526.

Yu, T. W., 2003: Operational use of QuikSCAT winds in NCEP GDAS. Preprints, *12th Conf. on Satellite Meteorology and Oceanography,* Long Beach, CA, Amer. Meteor. Soc., CD-ROM, JP4.7.

Yuan, X., 2004: High wind evaluation in the Southern Ocean. *J. Geophys. Res.,* **109,** D13101, doi:10.1029/2003JD004179.